Journal of the European Ceramic Society 22 (2002) 2283–2289
www.elsevier.com/locate/jeurceramsoc

Thermal decomposition of cerium(III) acetate studied with sample-controlled thermogravimetric–mass spectrometry (SCTG—MS)

Tadashi Arii[a,*], Takeyoshi Taguchi[b], Akira Kishi[c], Makoto Ogawa[d], Yutaka Sawada[d]

[a]*Thermal Analysis Division, Rigaku Corporation, 3-9-12 Matsubara, Akishima, Tokyo 196-8666, Japan*
[b]*X-ray Diffraction Division, Rigaku Corporation, 3-9-12 Matsubara, Akishima, Tokyo 196-8666, Japan*
[c]*X-ray Research Laboratory, Rigaku Corporation, 3-9-12 Matsubara, Akishima, Tokyo 196-8666, Japan*
[d]*Department of Applied Chemistry, Faculty of Engineering, Tokyo Institute of Polytechnics, 1583 Iiyama, Atsugi, Kanagawa 243-0297, Japan*

Received 3 August 2001; accepted 29 December 2001

Abstract

Thermal decomposition of cerium(III) acetate hydrate, $Ce(CH_3CO_2)_3{\cdot}1.5H_2O$, to cerium(IV) oxide, CeO_2, in helium has been successfully investigated by sample-controlled thermogravimetry combined with evolved gas analysis by mass-spectrometry (SCTG–MS). Cerium(III) anhydrous acetate decomposed to cerium (IV) oxide through four decomposition steps in the temperature range of 250–800 °C. SCTG–MS was very useful to distinguish the successive decomposition accompanying the formation of the intermediate products to identify simultaneous gas evolution during the mass losses. The decomposition intermediates quenched from SCTG were characterized by X-ray diffraction (XRD) and X-ray absorption near-edge structure (XANES). The XANES revealed clearly the coexistence of Ce(III) and Ce(IV) and the valence change from cerium(III) to cerium(IV). The three decomposition intermediate products were presumed to be $Ce_2O(CH_3CO_2)_4$, $Ce_2O_2(CH_3CO_2)_2$ and $Ce_2O_2CO_3$. A detailed thermal decomposition mechanism of $Ce(CH_3CO_2)_3{\cdot}1.5H_2O$ is discussed.

Keywords: $Ce(CH_3CO_2)_3{\cdot}1.5H_2O$; CeO_2; SCTG–MS; Thermal decomposition; XANES

1. Introduction

Thermal decomposition of inorganic or organic crystalline salt hydrates is categorized to an important class of reactions that should be studied for a variety of potential applications to ceramic industries. For typical examples, low temperature synthesis via sol-gel process and/or thermal decomposition of metal-organic precursors has been widely used in various fields. Since the properties of oxide ceramics are greatly influenced by the precursor materials and their synthesis, a clarification of the formation reaction is indispensable for optimizing the manufacturing process as well as collecting the fundamental data. Fine oxide powders are often synthesized by thermal decomposition of various metal-organic salts. Many metal acetates are water-soluble and synthesized easily, so that they are applied to prepare oxide thin films by a wide range of techniques, such as metal-organic chemical vapor deposition, spray pyrolysis, sol-gel and dip coating or spin coating processes followed by thermal process at a relatively low temperature. It is therefore extremely meaningful to elucidate the thermal decomposition pass-way of metal acetates in detail.

Cerium(IV) oxide (called ceria), CeO_2, has a fluorite structure and is an important material with good mechanical, chemical and thermal stabilities. It has been widely used for polishing and decolorizing glass: rare-earth-doped ceria is recently investigated as a low-temperature solid-state electrode for fuel cell and oxygen sensors. Thin films of ceria has been used as optical coatings, heat mirrors, buffer materials for epitaxial high-temperature superconducting oxide films on various substrates and insulating layers.[1] Usually CeO_2 is prepared by ignition of cerium salts. Several studies of the thermal decomposition of rare-earth acetates have been reported in the literature[2–5] but the data for the cerium(III) acetate hydrates were often divergent. One of the present authors reported thermogravimetric analysis (TG) of cerium(III) anhydrous acetate under an inert atmosphere and new intermediate products.[6]

* Corresponding author. Fax.: +81-42-544-9650.
E-mail address: t-arii@rigaku.co.jp (T. Arii).

0955-2219/02/$ - see front matter
PII: S0955-2219(02)00019-5

Recently, the present authors reinvestigated the thermal decomposition of cerium(III) acetate hydrate in helium atmosphere using two novel thermal analyses; simultaneous analyses of thermogravimetric–differential thermal analysis–mass spectrometry (TG–DTA–MS) and simultaneous analyses of X-ray diffractometry – differential scanning calorimetry (XRD–DSC).[7] To study the underlying mechanism, such complementary experimental techniques based upon these three-dimensional thermal analyses decreased successfully the ambiguities in the data interpretation. The decomposition of cerium(III) anhydrous acetate to cerium(IV) oxide proceeded through four steps. The mass loss in the first step decreased remarkably with increasing the heating rate. Three intermediates including oxycarbonate were found when heated slowly with a constant heating rate in a series of linear heating TG (LHTG) experiments and/or LHTG under reduced pressure, in which the influence of the evolved gases on the decomposition rate is supposed to be negligible.

In case of conventional thermal analysis, the sample is forced to heat up at a constant rate, ignoring whether a certain change occurs or not in the sample, so that the thermal change process occurring in the sample is observed over a relatively wide temperature range. In same cases, the reaction initiated at the low temperature does not terminate at the higher temperature, where the next reaction begins simultaneously. In order to overcome such drawback of conventional constant rate heating, a few decades ago sample-controlled thermal analysis (SCTA or controlled-rate thermal analysis, CRTA) was invented independently by Paulik and Raquerol et al.[8] in which the rate change of the sample property (or the rate of reaction) is maintained to be constant in some modes by controlling the sample temperature. This just corresponds to the reverse concept of conventional thermal analysis. By SCTG the heating rate is reduced when the change of mass loss begins, so that the resolution is improved and high-temperature parallel reactions cannot occur. Recently, a sample-controlled thermogravimetry (SCTG) instrument is commercially available.[9–12] It is now applied to many fields, such as dehydration processes, and solid reactions and sintering. Sometimes, the mass loss curves of SCTG are quite different from those obtained by LHTG.[11,13]

The aim of this paper is to analyze the thermal decomposition of $Ce(CH_3CO_2)_3{\cdot}1.5H_2O$ to CeO_2 in inert atmosphere, and to propose an overall decomposition mechanism. In the present study, the thermal behavior of $Ce(CH_3CO_2)_3{\cdot}1.5H_2O$ in helium flow was investigated by means of simultaneous measurements that consist of SCTG and evolved gas analysis using mass spectrometer (SCTG–MS). The specimens quenched from various temperatures in the heating process were characterized by X-ray absorption near-edge structure (XANES).

2. Experimental

2.1. Specimen

The powder samples of cerium acetate(III) hydrate ($Ce(CH_3CO_2)_3{\cdot}1.5H_2O$, purity 99.9%, Rare Metallic Co. Inc.), cerium(III) carbonate octahydrate ($Ce_2(CO_3)_3{\cdot}8H_2O$, purity 99.99%, Kanto Chemical Co. Inc.) and cerium(III) oxide (CeO_2, purity 99.99%, Kanto Chemical Co. Inc.) were the commercially available reagent samples and used without any further purification. X-ray diffraction spectra showed only crystalline $Ce(CH_3CO_2)_3{\cdot}1.5H_2O$,[14] $Ce_2(CO_3)_3{\cdot}8H_2O$[15] and CeO_2,[16] respectively.

2.2. Apparatus

Thermogravimetric-differential thermal analysis, TG–DTA, was performed by a Rigaku Thermo Plus 8120D system with SCTG as described in more detail elsewhere for a similar apparatus.[12,13] The rate of mass loss was kept at an arbitrary constant value. A sequence of experiments was carried out with a fully automated and computerized SCTG system. The specimen (approximately 10 mg) was weighed into an open platinum crucible, and was heated up to 950 °C in high-purity helium (99.99%) with a flow rate of 200 ml/min, or in vaccuo (500 Pa).

The spectra of the gaseous products evolved from the specimen in TG–DTA (or SCTG) are simultaneously monitored with a quadrupole mass spectrometer (Q-MS; Model Thermo Mass, Rigaku). Thermo mass system is connected to TG–DTA via a gas interface system with 1100 mm-long fused silica capillary of an internal diameter of 0.075 mm. Details of the TG–DTA–MS equipment were described elsewhere.[12,17] All transfer pathway was kept at 250 °C to prevent condensation. The acceleration voltage of the ionization was fixed at potential of 70 eV. Detection mass region of m/z was fixed at 10–80. In a series of the simultaneous SCTG–MS experiments, to ignore desorption of any components adsorbed in the reference material such as α-Al_2O_3, only empty platinum crucible was prepared as reference.

The crystal structures of the specimens quenched from arbitrary temperatures in SCTG experiments were confirmed by X-ray diffractometer (XRD; Model RINT2500/PC, Rigaku) with graphite-monochromated CuK_α radiation ($\lambda = 1.5405$Å). A line shape X-ray source was operated at 50 kV and 40 mA and the data were collected in the range of $2\theta = 5$ to 90° with an interval of 0.02° and a scan speed of 2°/min.

X-ray absorption near-edge spectrum measurements were carried out with laboratory XAFS facility (Model; R-XAS Looper spectrometer, Rigaku) at room temperature on the cerium L_{III}-edge for the specimen

quenched from various temperatures. The resolution of the Ge(311) monochromator at the cerium-edge was 0.7 eV with an X-ray source size at the target of 12 mm (vertical) × 0.6 mm (horizontal). The X-ray generator operated at 16 kV and 50 mA producing a photon flux of about 10,000 cps at the sample. XANES region is scanned at 1 eV step over 100 eV and X-ray photons are counted 30 s at each step. Total data collection times were just less than 1 h.

3. Results and discussion

3.1. SCTG–MS analysis

Typical TG curves for $Ce(CH_3CO_2)_3{\cdot}1.5H_2O$ at 0.5 °C/min in helium flow and at 10 °C/min in vacuo are shown in Fig. 1. The thermal decomposition seems to proceed through five steps as numbered in the figure, but the plateau on the TG curves is clear only in case of the first step corresponding to dehydration terminated at 150 °C. After dehydration, the mass losses for the second to 5th steps at the inflection points resolved from the maximum between the DTG peaks are 14.2% at 287 °C, 14.6% at 304 °C and 8.4% at 355 °C, respectively, when heated at 0.5 °C/min in helium. The total mass loss reaches 50.0% at its final point (800 °C) and corresponds to the theoretical value (49.99%) to form cerium(IV) oxide. Elucidation of the decomposition mechanism is relative easy by TG with slow heating rate and/or in vacuo, where the evolved gases escape immediately from the specimen pan. The plateaus on the both TG curves intersect at the mass loss of 14.5% which is slightly higher than that 14.2% determined by the inflection point. Results of SCTG are shown in Fig. 2 as function of time. The sample was heated at a constant heating rate of 5 °C/min until a predetermined switch-over temperature of 180 °C, above which the mass loss rate was kept at 0.06%/min by SCTG mode of the automatic heating/cooling control. The temperature changed smoothly and dramatically as seen in the figure with the pre-selected mass loss rate. Several discontinuities were observed in the temperature curve, as inflection points, up to 49.9% mass loss. These inflectional and stepwise changes indicate the multiple reaction. SCTG with different mass loss rates (0.04–0.1%/min) showed approximately the same curves as those in Fig. 2.

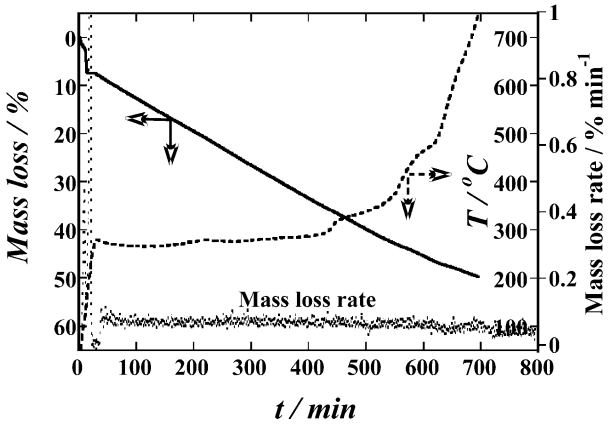

Fig. 2. SCTG curve of $Ce(CH_3CO_2)_3{\cdot}1.5H_2O$ at mass loss rate of 0.06%/min.

Fig. 3 illustrates the SCTG curve in helium flow as a function of temperature. In this figure, the results of Fig. 1 are superimposed for reference. The decomposition steps were significantly indicated compared with the results of constant heating rate. Thus, it is clear that SCTG improved effectively the resolution of the mass loss curve. The SCTG separated successfully the second and the third decomposition steps (14.3 and 14.6%, respectively), although the both steps proceed at approximately same temperature. The clear separation of these steps should be interpreted as the sequential

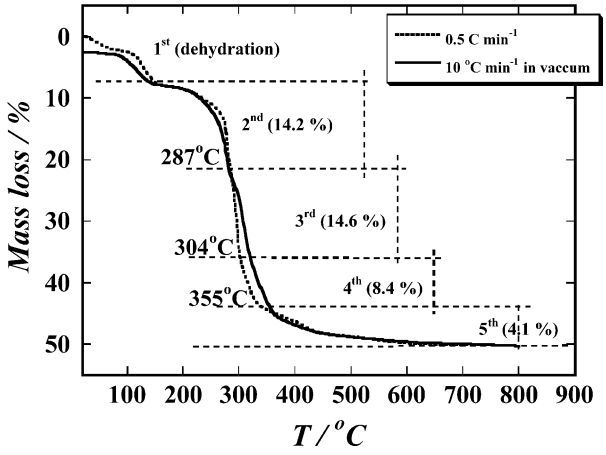

Fig. 1. TG–DTA curves of $Ce(CH_3CO_2)_3{\cdot}1.5H_2O$ using 0.5 °C/min in helium and 10 °C/min in vacuo.

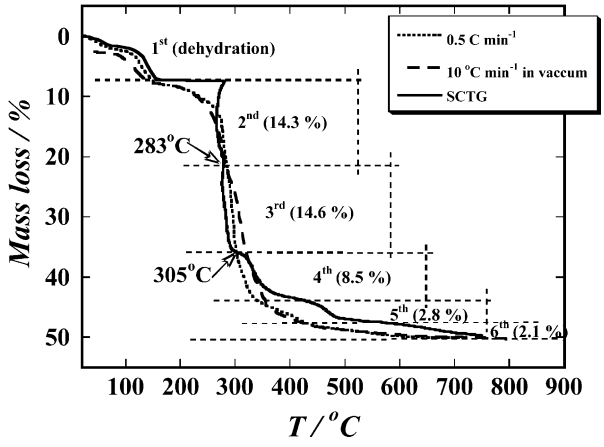

Fig. 3. Comparison of mass loss curves of $Ce(CH_3CO_2)_3{\cdot}1.5H_2O$ using LHTG of 0.5 °C/min in helium and 10 °C/min in vacuo with SCTG at 0.06%/min in helium.

reactions; the simultaneous parallel reaction observed when heated rapidly would result from the inhomogeneous temperature or the inhomogeneous partial pressure of the evolved gases in the sample pan. The mass loss (14.3%) for the second step agreed satisfactorily with that (14.5%) determined by the intersection of TG curves. The fourth step (8.5%) was well-defined by the plateau in SCTG. The 5th step in the LHTG was divided into the fourth and the 5th steps (2.8 and 2.1%, respectively).

Fig. 4 shows the results of SCTG–MS, and Fig. 5 illustrates the mass spectra of the gases detected at 267, 281, 342, 467 and 641 °C, where the temperature corresponds to each middle point in the second to 6th decomposition steps, respectively. The mass spectra of the evolved gas during the second to fourth decomposition steps were similar to each other, except that the relative intensity of m/z 44 ion in the fourth decomposition step is negligibly weak. The gases evolved were identified as a mixture of acetone (m/z 15, 43 and 58)[18] and carbon dioxide (m/z 12, 16, 28 and 44),[19] by comparing with mass spectra in NIST chemical and structural database; the other week ions agreed approximately to the fragmentation ions of acetone. Similarly, the gas evolved in the 5th decomposition step was interpreted as a mixture of carbon monoxide (m/z 12,16 and 28)[20] and carbon dioxide. Formation of carbon monoxide is highly probable because the relative intensity of m/z 28 was higher than that (11.7%) expected from the fragmentation of carbon dioxide. The gas evolved in the final 6th decomposition step was assigned to carbon monoxide. Fig. 6 shows the mass chromatograms of m/z 18, 28, 44 and 58 ions, which correspond to the molecular ions for the above identified gases. The intensities of m/z 58 (acetone) and 44 (carbon dioxide) were approximately proportional during the second to fourth decomposition steps to each other, while the intensity of m/z 44 decreased dramatically in the fourth step.

The above in mind, in the 2nd to 4th decomposition steps, a tentative decomposition scheme as follows is proposed assuming that evolution of carbon dioxide during the fourth step is negligible.

$$2Ce(CH_3CO_2)_3 \rightarrow Ce_2O(CH_3CO_2)_4 + (CH_3)_2CO + CO_2 \quad (2nd)$$

$$Ce_2O(CH_3CO_2)_4 \rightarrow 2CeO(CH_3CO_2) + (CH_3)_2CO + CO_2 \quad (3rd)$$

$$Ce_2O_2(CH_3CO_2)_2 \rightarrow Ce_2O_2CO_3 + (CH_3)_2CO \quad (4th)$$

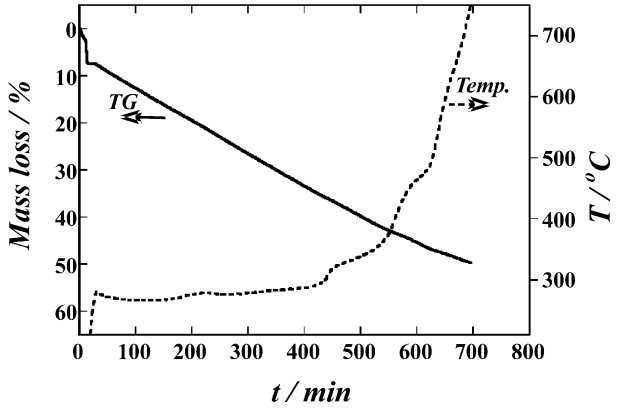

Fig. 4. Results of SCTG–MS curves as function of time.

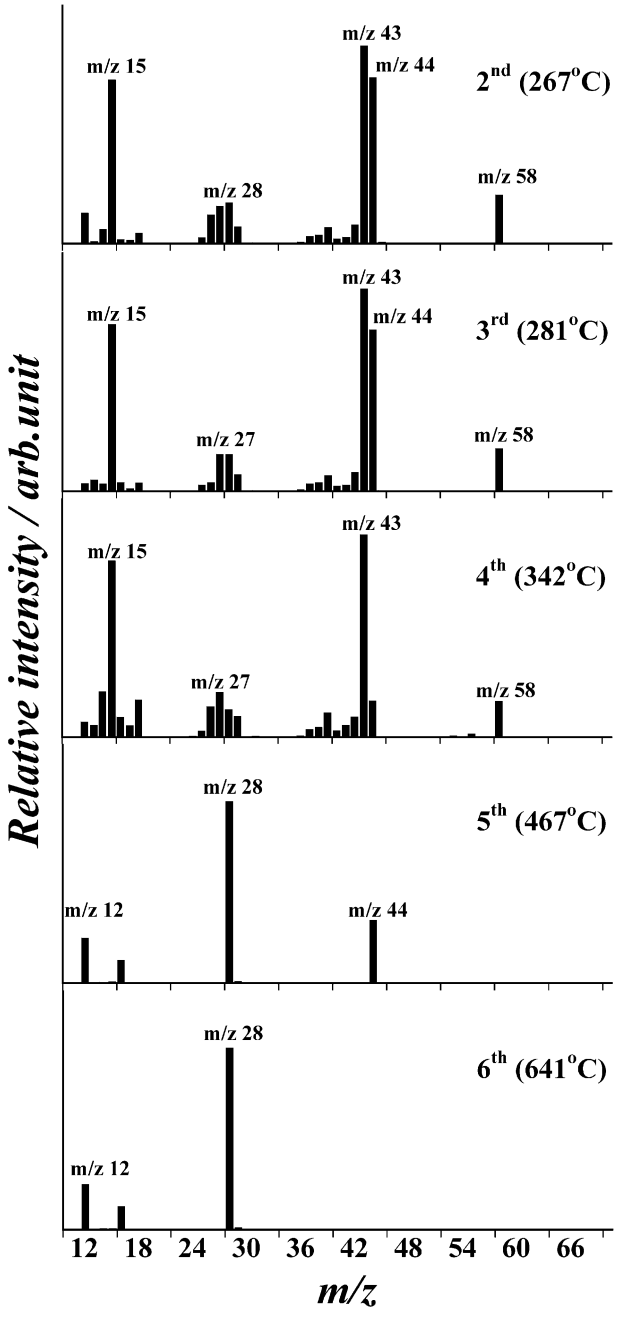

Fig. 5. Mass spectra at between 250 and 800 °C.

The theoretical mass losses (14.83, 14.83 and 8.44%) agreed satisfactory with the observed SCTG values (14.3, 14.6 and 8.5%). This agreement supposed the decomposition scheme of the previous paper.[7] However, the subsequent decomposition steps (the 5th and the 6th) were different as will be discussed later.

As mentioned above, the gases evolved during the 5th and 6th decomposition steps were attributed to carbon monoxide and the small amount of carbon dioxide. The m/z 28 can be detected in case of carbon dioxide. However, carbon monoxide was detected during all over the 5th and the 6th steps, while carbon dioxide was hardly detected in the 6th step, and the change of the relative intensities of m/z 28 and 44 in Fig. 6 did not synchronize to each other. These results suggest that carbon monoxide was predominant during both decomposition steps.

3.2. XRD analysis

In order to understand the decomposition mechanism, it is important to identify the intermediates formed in the solid phase. Fig. 7 shows a comparison of the XRD diagrams for the intermediate products quenched immediately from the temperatures (540 and 800 °C) at which the 5th and the 6th decomposition steps completed on SCTG. The XRD spectra showed only crystalline CeO_2,[16] except for the crystallinity. Consequently, the presumed composition $Ce_2O_2CO_3$ should be directly decomposed to cerium(IV) oxide accompanied by the evolution of CO, as tentatively indicated as follows.

$$Ce_2O_2CO_3 \rightarrow CeO_2 + CO \quad \text{(5th)}$$

The following reaction is negative because crystalline Ce_2O_3[21] was absent.

$$Ce_2O_2CO_3 \rightarrow Ce_2O_3 + CO_2$$

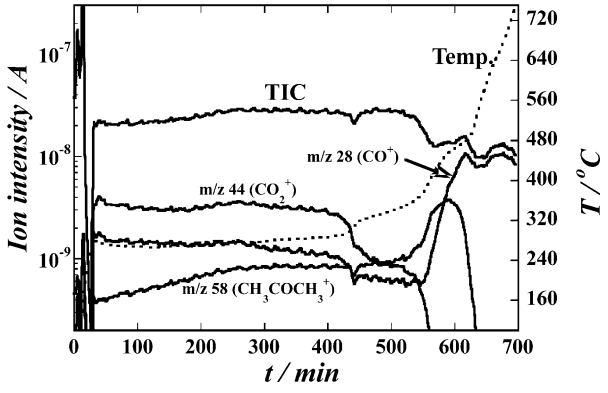

Fig. 6. Mass chromatograms of characteristic ions (m/z 28, 44 and 58) m/z 28, CO; m/z 44, CO_2; m/z 58, $(CH_3)_2CO$.

However, the above interpretation fails to explain the production of the small amount of CO_2 evolved in the 5th stage.

3.3. Thermal decomposition of cerium(III) carbonate

Manabe et al.[6] proposed that the intermediate products after the second and the third steps to be $(Ce(CH_3CO_2)_3)_x{\cdot}(Ce_2O_3)_y$ because if IR absorption assigned to CH_3COO^-, while CO_3^{2-} was undetected. The intermediate products after the fourth step was assumed to be $(Ce_2(CO_3)_3)_x{\cdot}(Ce_2O_3)_y$, because of the detection of CO_3^{2-}, while CH_3COO^- was absent.

An origin of CO_2 evolved in the 5th step was examined experimentally by TG–DTA–MS for the thermal decomposition of cerium(III) carbonate octahydrate $Ce_2(CO_3)_3{\cdot}8H_2O$. Fig. 8(a) shows the result of TG–MS heated at 10 °C/min in helium flow. After dehydration ($8H_2O$) the decomposition consists of several stages, cerium(III) anhydrous carbonate was completely decomposed through two consecutive reaction steps accompanying an evolution of CO_2 and a small amount of CO. The mass loss reaches 42.2% at around 900 °C and corresponds to the theoretical value (43.04%) to form cerium(IV) oxide. The mass chromatograms (m/z 18, 28 and 44 ions corresponding to H_2O^+, CO^+, CO_2^+, respectively) are also shown in this figure, where the m/z 28 was plotted the ion intensity after subtracting the CO^+ fragmentation from CO_2. The evolution of CO was clearly observed before the evolution of CO_2. The peak-top temperatures on the chromatogram curves of CO_2 and CO were 474 and 505 °C, respectively. The most probable decomposition scheme of cerium(III) anhydrous carbonate $Ce_2(CO_3)_3$ was proposed as follows:

$$Ce_2(CO_3)_3 \rightarrow Ce_2O_2CO_3 + 2CO_2$$

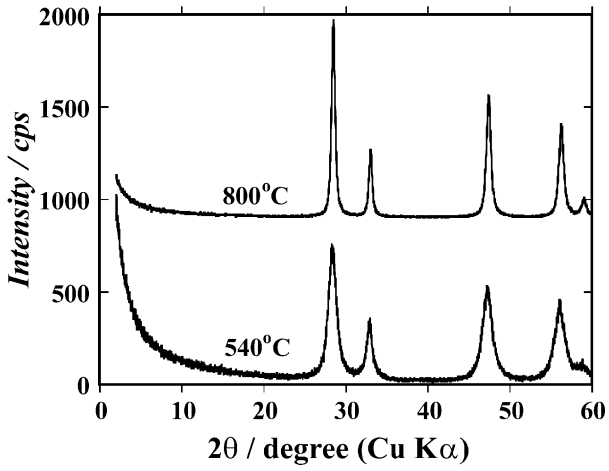

Fig. 7. Comparison of XRD diagrams for decomposition products of cerium(III) anhydrous acetate quenched from 540 and 800 °C using SCTG of 0.06%/min.

$$Ce_2O_2CO_3 \rightarrow CeO_2 + CO$$

Moreover, Fig. 8(b) illustrates a comparison of $Ce_2(CO_3)_3$ with $Ce(CH_3CO_2)_3$ in helium flow at 10 °C/min. The temperatures of gas evolution agreed satisfactorily with those of the 5th decomposition step of $Ce(CH_3CO_2)_3$.

From this finding, we conclude that CO_2 evolved in the 5th stage is attributed to the decomposition of small amount of $Ce_2(CO_3)_3$ contained in the intermediate product $Ce_2O_2CO_3$.

3.4. XANES analysis

X-ray absorption at the rare-earth L_{III}-edge has proven to be a straightforward and reliable tool for identifying the rare-earth valence in a variety of materials, including mixed-valence systems having either a homogeneous or imhomogeneous distribution of two distinct, integrally occupied 4*f* shells. Fig. 9 compares the Ce L_{III}-edge XANES spectra of the specimens quenched from different temperatures (200, 283, 315, 400, 540 and 800 °C, respectively), along with a standard spectrum of crystalline CeO_2 in cubic phase. Each temperature corresponds to that of the end of each decomposition stage on CRTG curve. The spectra are approximately distinguished to three temperature groups; (a) 200 and 283 °C, (b) 315 and 400 °C and (c) 540, 800 °C and CeO_2.

The pre-edge structure, labeled A, is assigned to final states with delocalized *d* character at the bottom of the conduction band. Due to the cubic crystal-field splitting of Ce 5*d* states, labeled B and D features are associated to the transitions of Ce $2p \rightarrow$ Ce $4f^1 5de_g\underline{L}$ and Ce $2p \rightarrow$ Ce $4f^1 5dt_{2g}\underline{L}$, where, L denotes an oxygen ligand *2p* hole; $4f^1$ refers to an electron from an oxygen orbital to a cerium *4f* one (charge transfer-like).[24] The labeled E feature is attributed to the contribution of a different final state configuration Ce $2p \rightarrow$ Ce $4f^0 5d$. The spectra of the specimens quenched from 540 and 800 °C are similar to each other and agreed approximately with the spectral features of CeO_2 in cubic phase which are characterized by the peak A, B, D and E. The cerium in the specimens quenched from 315 and 400 °C showed an increase of Ce^{4+}, indicated by the E feature peak in the specimen, and showed that Ce^{3+} and Ce^{4+} coexist. The cerium in the specimen quenched from 540 °C are mainly Ce^{4+}, since the spectrum superimposes with that of CeO_2 standard. The product quenched from 200 °C corresponds to an amorphous cerium(III) anhydrous acetate, $Ce(CH_3CO_2)_3$. Both the Ce L_{III}-edge spectra of tetravalent CeO_2 and trivalent $Ce(CH_3CO_2)_3$ quenched from 200 °C were in agreement with the results of previous works.[22,23] For the Ce L_{III} edge spectrum of $Ce(CH_3CO_2)_3$ quenched from 200 °C, the strongest peak at C, characterizes the Ce in trivalent state and completely different from the spectrum of standard CeO_2 due to the dipole-allowed transition of Ce $2p \rightarrow$ Ce $4f^1 5d$ final states. The similarity of the spectra for the

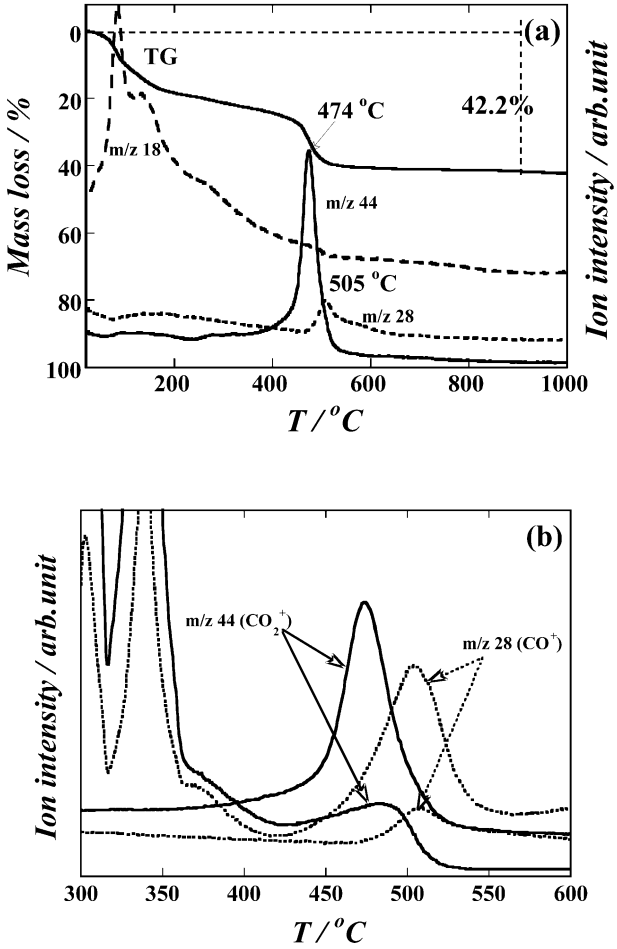

Fig. 8. TG–MS results of $Ce_2(CO_3)_3 \cdot 8H_2O$ and comparison of evolution behavior of CO and CO_2 compared with those of decomposition of $Ce(CH_3CO_2)_3$.

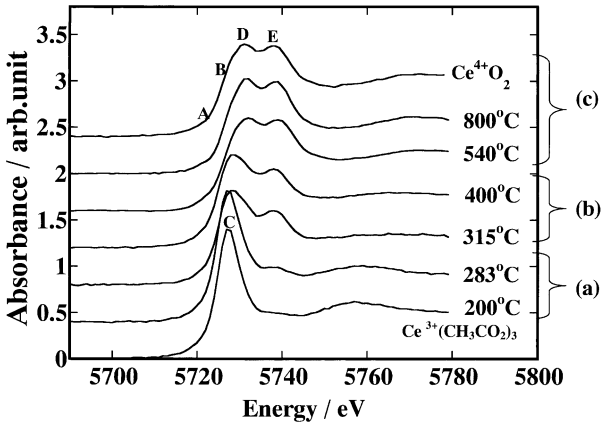

Fig. 9. The normalized Ce L_{III}-edge XANES spectra of the specimens at different quenching temperatures, along with standard spectra of crystal CeO_2.

specimens quenched from 283 and 200 °C is evident, except for the small amount of absorption corresponding to E feature. Both are dominated by a single peak C above the trivalent absorption determined from the trivalent cerium acetate. The cerium in the specimen quenched from 283 °C is interpreted as mainly Ce^{3+} with less Ce^{4+}. Although the spectra of the specimens quenched from 315 and 400 °C are also similar to each other, the height of the second peak corresponding to E feature increased slightly with proceeding of the decomposition; their spectra seem to be just a fingerprint mixed trivalent and tetravalent cerium valence states. Wan et al. showed that Ce L_{III}-edge spectra obtained from different proportional mixtures of the model compounds $CeCl_4{\cdot}7H_2O$ and CeO_2, providing references for Ce^{3+} and Ce^{4+}, are useful to recognize and discriminate the cerium valence states in the specimens.[25] Since the height of the peak E increases proportionally, with increasing CeO_2 content, information on the constitution of the specimens can be determined by direct observation of the edge shape of the spectra.

Based on the above results, we concluded that a valence change from Ce^{3+} to Ce^{4+} occurred with proceeding the decomposition of cerium(III) anhydrous acetate and was approximately completed at 540 °C. The Ce^{4+} was detected in the quenched specimens mainly consisted of two cerium oxyacetates ($Ce_2O(CH_3CO_2)_4$, $CeO(CH_3CO_2)$) and cerium oxycarbonate $Ce_2O_2CO_3$.

4. Conclusions

Thermal decomposition of $Ce(CH_3CO_2)_3{\cdot}1.5H_2O$ to cerium (IV) oxide in helium was investigated by SCTG–MS and XANES for the specimens quenched from the decomposition stages obtained by SCTG. The SCTG provided a more simplified information to understand the reaction mechanism without reducing the pressure. The mass loss steps were successfully separated by SCTG. The each mass loss step in a narrow temperature region was characterized by simultaneously identification of the evolved gases by mass spectrometer. Evolution of acetone, carbon dioxide and carbon dioxide were detected. Cerium(III) anhydrous acetate, $Ce(CH_3CO_2)_3$, decomposed to CeO_2 via $Ce_2O(CH_3CO_2)_4$, $Ce_2O_2(CH_3CO_2)_2$ and $Ce_2O_2CO_3$. Coexisted valence states of Ce^{3+} and Ce^{4+} in these intermediate products were detected by XANES. A valence change from Ce^{3+} to Ce^{4+} initiated at the decomposition of cerium(III) anhydrous acetate and was completed above 540 °C.

These results proved that SCTG-MS and XANES are straightforward and reliable tools for determining the decomposition mechanism in detail to understand complicated reaction processes during syntheses of advanced ceramic materials.

References

1. Windholz, M. *et al.*, ed., *The Merck Index*, 8th edn. Merck & Co., Inc., Rah, 1968.
2. Maksimov, V. N. and Semenenko, K. N., *Z. Neorg. Khim.*, 1958, **3**, 1468–1471.
3. Michalina, D. and Maria, K., *Ann. Univ. Material Curie-Sklodowska, Sect AA*, 1971, **26**, 341–358.
4. Mayer, I. and Kassierer, F., *J. Inorg. Nucl. Chem.*, 1966, **28**, 2430–2432.
5. Edwards, D. A. and Hayward, R. N., *Can. J. Chem.*, 1968, **46**, 3343–3346.
6. Manabe, K. and Ogawa, M., *Nihonkagakukaishi*, 1983, **7**, 1092–1095, in Japanese.
7. Arii, T., Kishi, A., Ogawa, M. and Sawada, Y., *Analytical Sciences*, 2001, **17**, 875–880.
8. Rouquerol, J., *Thermochim. Acta*, 1989, **144**, 209–224.
9. Arii, T., Senda, T. and Fujii, N., *Thermochim. Acta*, 1995, **267**, 209–221.
10. Arii, T., Terayama, K. and Fujii, N., *J. Therm. Anal.*, 1996, **47**, 1649–1661.
11. Arii, T. and Fujii, N., *J. Anal. Appl. Pyrolysis*, 1997, **39**, 129–143.
12. Arii, T., Sawada, Y., Kieda, N. and Seki, S., *J. Mass Spectrum. Soc. Jpn*, 1999, **47**, 354–359.
13. Arii, T., Nakagawa, H., Ichihara, Y. and Fujii, N., *Thermochim. Acta*, 1998, **319**, 139–149.
14. Entry No.26–345, ICDD (Cerium(III) acetate hydrate, $Ce(CH_3CO_2)_3{\cdot}1.5H_2O$).
15. Entry No.38–377, ICDD (Cerium(III) carbonate octahydrate, $Ce_2(CO_3)_3{\cdot}8H_2O$).
16. Entry No. 81–792, ICDD (Cerium(IV) oxide, CeO_2).
17. Arii, T. and Masuda, Y., Thermochim. *Acta*, 1999, **342**, 139–146.
18. Entry No. 125, NIST 107 (Acetone, $(CH_3)_2CO$).
19. Entry No. 36, NIST 107 (Carbon dioxide, CO_2).
20. Entry No. 8, NIST 107 (Carbon monoxide, CO).
21. Entry No. 78-484, ICDD (Cerium(III) oxide, Ce_2O_3).
22. Capehart, T. W., Mishra, R. K. and Herbst, J. J., *J. Appl. Phys.*, 1992, **72**, 676–679.
23. Kaindl, G., Schmiester, G. and Sampathkumaran, E. V., *Phys. Rev. B*, 1988, **38**, 10174–10177.
24. Soldatov, A. V. and Ivanchenko, T. S., *Phys. Rev. B*, 1994, **50**, 5074–5080.
25. Wan, J., Thompson, G.E., Ng, T. K., Lu, K. Q. and Smith, C. J. E., J. Phys. IV France, 1997, **7**, 1183–1184.